

Global Flows in Quantum Gravity

N. Christiansen,¹ B. Knorr,¹ J. M. Pawłowski,^{1,2} and A. Rodigast¹

¹*Institut für Theoretische Physik, Universität Heidelberg, Philosophenweg 16, 69120 Heidelberg, Germany*

²*ExtreMe Matter Institute EMMI, GSI Helmholtzzentrum für Schwerionenforschung mbH, Planckstr. 1, 64291 Darmstadt, Germany*

We study four-dimensional quantum gravity using non-perturbative renormalization group methods. We solve the corresponding equations for the fully momentum-dependent propagator, Newtons coupling and the cosmological constant. For the first time, we obtain a global phase diagram where the non-Gaussian ultraviolet fixed point of asymptotic safety is connected via smooth trajectories to a classical infrared fixed point. The theory is therefore ultraviolet complete and deforms smoothly into classical gravity as the infrared limit is approached.

I. INTRODUCTION

Understanding the quantization of the gravitational force is an outstanding problem in theoretical physics. Any viable theory of quantum gravity must connect stable infrared (IR) physics with a well-behaved ultraviolet (UV) limit. The asymptotic safety scenario provides a UV-completion in a natural way. It is based on a non-Gaussian UV fixed point, which leads to vanishing β -functions in the limit of arbitrarily high energy scales and renders the couplings finite even beyond the Planck scale [1].

The asymptotic safety scenario received growing attention during the past decades and has been studied with different methods. The underlying fixed point structure was found in the non-perturbative continuum approach [2–11], as well as in lattice simulations [12–14]. The former is based on the functional renormalization group, in particular on its formulation for the effective action [15]. The crucial UV fixed point is confirmed in various approximations, including the coupling to gauge and matter fields [16–21], dilaton gravity [22] and higher derivative calculations [23–27]. There is also a rich field of phenomenological applications based on asymptotically safe quantum gravity. This includes e.g. implications for the standard model and its extensions [28, 29], black hole physics [30–33], collider experiments [34, 35] and cosmology [36, 37]. However, the standard calculations lead to an ill-defined IR limit since the trajectories exhibit a singular behaviour on large length scales.

In [2] an IR fixed point has been found as the end-point of a singular line. The existence of this fixed point was only seen within a proper distinction of background and dynamical couplings. The singular behaviour in the vicinity of the IR fixed point was attributed to the approximation. The first smooth IR fixed point in asymptotically safe gravity, allowing for a theory that is well defined on all energy scales, was found in [3]. There, however, a non-classical behaviour in the vicinity of the IR fixed point has been computed, therefore leading to modified gravity on very large length scales. Again, the non-classical behaviour may be attributed to the approximation. Further discussions on this issue from different perspectives can be found in [38–41].

In the present work, we construct a qualitatively enhanced approximation within the systematic vertex expansion scheme introduced in [3]. With this enhanced approximation the theory is asymptotically safe in the UV, and exhibits an IR fixed point which describes classical gravity. The corresponding renormalization group (RG) trajectories are globally smooth. They connect the known IR physics with classical gravity on large length scales with a viable theory of Planckian and trans-Planckian gravity. The present scenario encodes that quantum gravity effects set in at about the Planck-scale, and are absent for energy-scales $E \ll M_{\text{Pl}}$.

This work improves the vertex expansion scheme set-up in [3] in several aspects. We compute, for the first time, fully momentum-dependent wave-function renormalizations for the graviton and the ghost. Note that the wave function renormalizations are functions of the covariant Laplacian, and hence this takes into account infinitely many terms in an expansion of the effective action in powers of the covariant derivative. Additionally, multi-graviton interactions are constructed from their scaling behaviour, see [42]: the dependence on the running RG-scale is deduced from consistent RG-scaling of the vertex. This novel self-consistent vertex construction is of major importance for the transition from UV to IR scaling, and the stability of the IR regime.

The present work is organized as follows: We introduce our approximation scheme in [section II](#), and the vertex construction in [section III A](#). The flow equations for the fully momentum-dependent propagators are derived in the subsequent subsections. The consistency analysis in [section III D](#) constrains the momentum-independent parts of the vertex functions, and is crucial for the global properties of the phase diagram. The latter is the topic of the first section of the results, [section IV A](#). Moreover, the reliability of all results is tested within a regulator study. To this end we use the optimized regulator as well as a class of exponential ones. The results are found to be stable against variations of the regulator. The properties of the UV regime are discussed in [section IV B](#). In this section we also investigate the stability and reliability of the derivative expansion, at the basis of the full momentum-dependence. In [section IV C](#) the properties of the IR regime are discussed.

II. FLOWS IN QUANTUM GRAVITY

A quantum field theory is entirely described by a complete set of correlation functions. The generating functional for the 1PI correlators is the effective action $\Gamma[\bar{g}, \phi]$, where we have already introduced a fixed background metric \bar{g} and a fluctuation super-field ϕ . In the case of gravity this super-field is given by the vector $\phi = (h, \bar{c}, c)$, where h is the graviton field and c, \bar{c} are the corresponding ghost and anti-ghost fields.

In the present work we use the functional renormalization group approach, for reviews on quantum gravity see [5–11], for general reviews and other applications see e.g. [43–57]. With the functional renormalization group, the effective action can be determined via a functional differential equation for the scale-dependent effective action $\Gamma_k[\bar{g}, \phi]$, which for quantum gravity is given by [4]

$$\begin{aligned} \partial_t \Gamma_k[\bar{g}, \phi] = & \frac{1}{2} \text{Tr} \left[\frac{1}{\Gamma_k^{(2h)} + R_{k,h}} \partial_t R_{k,h} \right] [\bar{g}, \phi] \\ & - \text{Tr} \left[\frac{1}{\Gamma_k^{(\bar{c}c)} + R_{k,c}} \partial_t R_{k,c} \right] [\bar{g}, \phi]. \end{aligned} \quad (1)$$

It involves an IR regulator R_k which is implemented on the level of the path integral and carries an IR cutoff-scale k . In addition to that, t denotes the logarithmic RG scale, $t := \log(k/k_0)$, with an arbitrary normalization scale k_0 , and the Tr implies an integral over all continuous and a sum over all discrete indices. We will also make use of the notation $\partial_t f(k) =: \dot{f}(k)$ for any scale-dependent quantity. Moreover, we have introduced the notation

$$\Gamma_k^{(\phi_1 \dots \phi_n)}[\bar{g}, \phi] := \frac{\delta^n \Gamma_k[\bar{g}, \phi]}{\delta \phi_1 \dots \delta \phi_n} \quad (2)$$

for the 1PI vertex functions, which are derivatives of the effective action with respect to the fluctuation fields and are the elements of the full super space matrix $\Gamma_k^{(n)}$.

The right hand side of the flow equation (1) depends on the two-point correlators of the fluctuation field ϕ . It is important to note that the fluctuation correlation functions do not agree with the background correlations, i.e.

$$\left. \frac{\delta^2 \Gamma_k[\bar{g}, \phi]}{\delta h^2} \right|_{\phi=0} \neq \frac{\delta^2 \Gamma_k[\bar{g}, 0]}{\delta \bar{g}^2}, \quad (3)$$

for details see [3, 19, 58–60]. In other words, one cannot extract dynamical couplings from the flow of the background field effective action at vanishing fluctuation fields, $\phi = 0$. This directly relates to the fact that the flow equation (1) for the effective action at $\phi = 0$ is not closed within the standard background field approach. More importantly, avoiding unphysical background contributions can be crucial for capturing the correct non-perturbative physics. In conclusion, in the FRG setup,

this strongly suggests to start from the exact equation for the inverse fluctuation propagator.

Moreover, the master flow equation (1) leads to an infinite hierarchy of coupled partial integro-differential equations for the scale-dependent vertex functions $\Gamma_k^{(n)}$. More precisely, the equation for the n -point vertex function contains vertex functions of order $n+1$ and $n+2$. This system is usually not exactly solvable. Therefore, one has to employ certain approximation schemes. We assume that the effective action can be expanded in a functional Taylor-series around the fixed background metric \bar{g} . Moreover, we choose the flat Euclidean metric, i.e. the identity $\bar{g}_{\mu\nu} = \delta_{\mu\nu}$, as the expansion point. We will need this expansion up to fourth order in the graviton field. In symbolic notation, the effective action takes the form

$$\begin{aligned} \Gamma_k[\bar{g}, \phi] = & \sum_n \frac{1}{n!} \Gamma_k^{(n)}[\bar{g}, 0] \phi^n \\ = & \Gamma_k[\bar{g}, 0] + \Gamma_k^{(h)}[\bar{g}, 0] h + \Gamma_k^{(2h)}[\bar{g}, 0] h^2 \\ & + \Gamma_k^{(3h)}[\bar{g}, 0] h^3 + \Gamma_k^{(4h)}[\bar{g}, 0] h^4 + \dots \\ & + \Gamma_k^{(\bar{c}c)}[\bar{g}, 0] \bar{c} c + \dots \end{aligned} \quad (4)$$

The first and second term are of order h^0 and h^1 and do not enter the RHS of the flow equations for any $\Gamma_k^{(n)}$.

The above expansion of the effective action in powers of the fluctuating field around a flat Euclidean background $\bar{g}_{\mu\nu} = \delta_{\mu\nu}$ also restricts the number of higher derivative operators which can contribute to the vertex functions of n -th order. For instance, the most general form of the two-point function derives from an action which includes at most $\mathcal{O}(R^2)$ operators. All higher order terms vanish after two functional differentiations and evaluation on a flat background. Terms with higher order than this only contribute to vertex functions of order $n > 2$.

III. VERTEX EXPANSION

In the present work we use the systematic vertex expansion scheme as suggested in (4). The hierarchy of flow equations that has been introduced in the last section has to be truncated at finite order. This means that one can calculate the flow of a vertex function of given order n and use an ansatz for $\Gamma_k^{(n+1)}$ and $\Gamma_k^{(n+2)}$. We will compute the basic quantity of the present approach, the full two-point correlation functions of the fluctuation fields ϕ , that is $n = 2$. The corresponding flows rely on the two- but also on the three- and four point functions of the fluctuation fields. Hence we also introduce approximations for $\Gamma_k^{(3)}$ and $\Gamma_k^{(4)}$ that are consistent with the symmetries of the theory and have the correct RG-scaling. The latter property is essential for the global UV–IR flows considered here.

A. Structure of the vertex functions

First of all, we have to specify the tensor structures of the vertices. In the present work, we use the classical tensor structures which arise from functional differentiation of the Einstein-Hilbert action. The gauge-fixed Einstein-Hilbert action, including the ghost part, is given by

$$S = \frac{1}{16\pi G_N} \int d^4x \sqrt{\det g} (-R + 2\Lambda) + \int d^4x \sqrt{\det \bar{g}} \bar{c}^\mu \mathcal{M}_{\mu\nu} c^\nu + \int d^4x \sqrt{\det \bar{g}} \frac{1}{2\xi} \bar{g}^{\mu\nu} F_\mu F_\nu. \quad (5)$$

In (5), G_N is the Newton constant and Λ is the cosmological constant. The Fadeev-Popov operator is given by

$$\mathcal{M}_{\mu\nu} = \bar{\nabla}^\alpha (g_{\mu\nu} \nabla_\alpha + g_{\alpha\nu} \nabla_\mu) - \bar{\nabla}_\mu \nabla_\nu, \quad (6)$$

and the linear gauge fixing conditions reads

$$F_\mu = \bar{\nabla}^\nu h_{\mu\nu} - \frac{1}{2} \bar{\nabla}_\mu h^\nu{}_\nu. \quad (7)$$

Moreover, in this work we restrict ourselves to Landau gauge, that is $\xi \rightarrow 0$. Extended ghost interactions are studied e.g. in [61, 62].

The standard Einstein-Hilbert truncation amounts to replacing the gravitational coupling and the cosmological constant in (5) by running couplings $G_{N,k}$ and Λ_k . The vertex functions are then given by functional derivatives of this effective action. However, this approximation turns out to be inconsistent in the physical IR limit, which will be discussed in detail later. We also mention that the basic Einstein-Hilbert truncation does not disentangle the difference between a wave-function renormalization and a running coupling, since the running of the latter is simply identified with the running of the former. Note that in Yang-Mills theory such an approximation gives a deconfining potential of the order parameter even in the confining regime, see [60, 63, 64]. In this case, it is also the non-trivial momentum-dependence of the correlation functions that plays a crucial rôle for capturing the correct non-perturbative physics. Additionally, in the UV limit, $k \rightarrow \infty$, the full momentum-dependence of correlation functions is potentially relevant. In particular, a derivative expansion implies $p^2/\text{scale}^2 \ll 1$ which relates to low energy physics. So far, these momentum-dependencies have not been taken into account.

Consequently, we construct more general vertex functions that take into account the above properties while keeping the classical tensor structures. The construction of such vertex expansions of the scale-dependent effective action was introduced in [42] and applied in the context of Yang-Mills theories. A similar truncation based on these ideas was recently applied in quantum gravity to [65]. One guiding principle in this construction is RG invariance, i.e. invariance of the full effective action under

a change of the renormalization scale μ :

$$\mu \frac{d}{d\mu} \Gamma = 0, \quad (8)$$

where μ should not be confused with the running IR cut-off scale k , for a detailed discussion see [48]. In addition to that, we parameterize the vertex functions, i.e. the coefficients in the expansion (4) schematically as

$$\Gamma^{(n)} = Z^{\frac{n}{2}} \bar{\Gamma}^{(n)} \quad (9)$$

with a μ -independent part $\bar{\Gamma}^{(n)}$ and a μ -dependent wave-function renormalization $Z(p^2)$ of the attached fields. The above construction implies the correct scaling behaviour for the fields according to

$$\mu \frac{d}{d\mu} \phi = \eta \phi. \quad (10)$$

In the present work we use a uniform wave function renormalization, $Z_h = Z_{h_i}$, for all components of the graviton. Non-uniform Z -factors will be subject to a forthcoming publication [66]. The transverse-traceless (TT) part of the full propagator is now parameterized as

$$\Gamma_{\text{TT}}^{(2h)}(p^2) = Z_h(p^2)(p^2 - M^2)\Pi_{\text{TT}}(p), \quad (11)$$

with the transverse-traceless projector $\Pi_{\text{TT}}(p)$, and an effective mass term M representing the momentum-independent part of the two-point function. Note that the Z -factors are functions of the covariant Laplacian Δ , and therefore include infinitely many terms in a covariant expansion of the effective action in powers of the Laplace operator. This is the first RG study of quantum gravity taking into account this general momentum dependence of the graviton and the ghost propagator. The fully momentum-dependent Z -factors lead to a vertex construction with the required RG scaling properties. They also embody a corresponding implicit, non-canonical momentum-dependence of the vertex functions, in line with the co-linear singularity structure of vertex functions. Note that a similar vertex construction is achieved by simply taking further h -derivatives of the two-point correlation function (11) with $p^2 \rightarrow \Delta(\bar{g}, h)$.

Finally, we allow for additional running parameters $\Lambda_k^{(n)}$ which govern the (consistent) scale-dependence of the momentum-independent part of the vertex functions. This takes into account scaling properties of the vertex functions that are crucial for the global flows structure, and has not been considered before. The construction of the vertex functions also include appropriate powers of a scale-dependent Newton coupling $G_{N,k}$ as prefactors of the vertex functions. These factors, apart from the wave function renormalization factors, encode the correct scale-dependence of the vertices, see [42]. Note that in general there are separate coupling constants $G_k^{(n)}$ for each vertex function, but we identify $G_k^{(n)} = G_{N,k}^{\frac{n}{2}-1}$ in the present work. Still, this construction goes far beyond

the approximations considered so far in RG-gravity. In summary, the vertex functions take the form

$$\Gamma_k^{(\phi_1 \dots \phi_n)} = \prod_{i=1}^n \sqrt{Z_{\phi_i, k}(p_i)} G_{N, k}^{\frac{n}{2}-1} \mathcal{T}_k^{(n)}(p_1, \dots, p_n; \Lambda_k^{(n)}), \quad (12)$$

with tensor structures

$$\mathcal{T}_k^{(n)} = S^{(n)}(p_1, \dots, p_n; G_N = k^2, \Lambda \rightarrow \Lambda_k^{(n)}), \quad (13)$$

that arise from functional differentiation of the classical Einstein-Hilbert action S given in (5). We left out the momentum arguments on the LHS as well as the functional dependence on the fields. If we leave out the functional argument, it is implicitly understood that the functional is evaluated at vanishing fluctuation fields and on a flat background. The tensor structures $\mathcal{T}_k^{(n)}$ carry not only the canonical explicit momentum-dependence of the vertex functions, but also the running parameters $\Lambda_k^{(n)}$. They are defined by

$$\mathcal{T}_k^{(n)}(p_i = 0; \Lambda_k^{(n)}) =: -2\Lambda_k^{(n)} \tilde{\mathcal{T}}^{(n)}(\delta_{\mu\nu}), \quad (14)$$

where $\tilde{\mathcal{T}}^{(n)}(\delta_{\mu\nu})$ is the tensor structure arising from functional differentiation of the integral of the volume form with respect to the metric tensor. The factor of -2 in the definition is introduced such that we recover the classical cosmological constant in the Einstein-Hilbert action. We emphasize again that the consistent RG-scaling of the parameters $\Lambda_k^{(n)}$ is of major importance for the transition from the UV regime to the IR regime, as well as for the stability of the IR regime. In this regime the $\Lambda_k^{(n)}$ are determined via a self-consistency analysis of the scaling behaviour. Details will be presented in the corresponding results sections.

An example for the above vertex construction is the scalar coefficient of the TT-two point function of the graviton,

$$Z_h(p^2)(p^2 - 2\Lambda_k^{(2)}), \quad (15)$$

see also (11). The tensor structures for the general two-point function, from which the above results via TT-projection, are given by (13) and arise from functional differentiation of the Einstein-Hilbert action. Equation (15) and (11) entail that $\Lambda_k^{(2)}$ is the effective graviton mass,

$$M_k^2 = -2\Lambda_k^{(2)}. \quad (16)$$

Once again, note that this mass term is not the cosmological constant.

B. Flow of the propagator

The flow of $\Gamma^{(2h)}$ in a standard Einstein Hilbert truncation has been calculated in [3]. The corresponding flow

FIG. 1: Diagrammatic representation of the flow of the second order vertex functions. The dressed graviton propagator is represented by a double line, the dressed ghost propagator by a dashed line, while a dressed vertex is denoted by a dot and the regulator insertion by a crossed circle.

equation is obtained by functional differentiation of (1), and its diagrammatic representation is shown in Figure 1.

In the present work, we compute the fully momentum-dependent two-point functions with the RG-consistent ansatz (12) for the three- and the four-point function. With Figure 1 and (12) the flows of the two-point functions $\Gamma^{(2)}$ depend on

$$(Z_h(p^2), Z_c(p^2), M^2, G_N, \Lambda^{(3)}, \Lambda^{(4)}). \quad (17)$$

Here we have already dropped the subscript k , and if not stated otherwise, all generalized couplings are scale-dependent.

The two-point function contains all tensor structures in the York transverse-traceless decomposition. The transverse-traceless part is not constrained by Slavnov-Taylor identities and is expected to carry the essential properties of the graviton. In this work we identify all wave function renormalizations of the graviton modes with that of the transverse-traceless mode. Hence, from now on, all expressions for the two-point functions relate to the TT-part. A study with all independent tensor structures will be presented elsewhere [66].

In this work, we use a regulator of the form $R_\phi(p^2) = Z_\phi(p^2)R_\phi^0(p^2)$ with $R_\phi^0(p^2) = p^2 r(p^2)\mathcal{T}_\phi$, where \mathcal{T}_ϕ denotes the tensor structure of the corresponding two-point function evaluated at vanishing mass, and $r(p^2)$ is a dimensionless shape function. Then, the flow of the inverse propagator reads

$$\begin{aligned} \partial_t \Gamma^{(2h)}(p^2) &= (p^2 + M^2) \partial_t Z_h(p^2) + Z_h(p^2) \partial_t M^2 \\ &= \text{Flow}^{(2h)}(p^2), \end{aligned} \quad (18)$$

where

$$\text{Flow}^{(2h)}(p^2) = G_N Z_h(p^2) \times \quad (19)$$

$$\int d^4 q \sum_\phi \left(\partial_t r(q^2) + \frac{\partial_t Z_\phi(q^2)}{Z_\phi(q^2)} r(q^2) \right) I_\phi(p^2, q^2, \Lambda^{(n)}).$$

In the above equation, $I_\phi(p^2, q^2, \Lambda^{(n)})$ are scalar functions that arise from the contraction of the diagrams and a subsequent projection onto the TT-structure, and $n = 2, 3, 4$. This structure follows from our vertex construction discussed above. Explicit expressions for the flow equations are given in Appendix A. For the ghost sector, we apply the same strategy and arrive at the much simpler equation

$$p^2 \partial_t Z_c(p^2) = \text{Flow}^{(\bar{c}c)}(p^2). \quad (20)$$

Note that with the RG consistent vertex ansatz (12) and the structure of the flow equations for $\Gamma^{(n)}$, one can infer that the wave-function renormalization $Z(p^2)$ does never enter a flow equation alone, but always in the combination \dot{Z}/Z . This motivates the definition of the anomalous dimensions of the graviton,

$$\eta_h(p^2) := -\frac{\partial_t Z_h(p^2)}{Z_h(p^2)}, \quad (21)$$

and of the ghosts,

$$\eta_c(p^2) := -\frac{\partial_t Z_c(p^2)}{Z_c(p^2)}. \quad (22)$$

We note that the RHS of the flow of the $\Gamma_k^{(2)}$ does depend on η_h, η_c, M^2 and the three- and four-point functions, see (17). In the standard Einstein-Hilbert setup, a scale-dependent gravitational coupling is constructed from the graviton wave-function renormalization, and the momentum-independent parts of the vertex functions are all identified with the cosmological constant, $\Lambda^{(n)} \equiv \Lambda$. This procedure closes the equations (18) and (20) and was used at least in parts in all FRG gravity calculations so far.

In the present work this identification, which spoils the scaling properties of the correlation functions, is avoided. For the gravitational coupling constant G_N , we use the relation of the present framework at flat backgrounds to that with geometrical effective actions, see [2]. This is discussed in more detail below. The couplings $\Lambda^{(n)}$ are constrained within a self-consistency analysis, see section III D.

Finally we introduce dimensionless, scale-dependent couplings, to wit

$$g := G_N k^2, \quad \mu := M^2 k^{-2}, \quad (23)$$

$$\lambda := \Lambda k^{-2}, \quad \lambda^{(n)} := \Lambda^{(n)} k^{-2}, \quad (24)$$

with $n \geq 3$ and $\Lambda = \Lambda^{(1)}$. It is left to project the functional flow onto individual flow equations for all running couplings.

1. The running mass

The flow equation for the mass M^2 is obtained from the flow of the inverse propagator, evaluated at the pole

of the propagator, i.e. $p^2 = -M^2$. Taking the t -derivative of the on-shell two-point function, $\Gamma^{(2h)}(-M^2)$, yields

$$0 = \partial_t \Gamma^{(2h)}(p^2) \Big|_{p^2 = -M^2} - Z_h(-M^2) \partial_t M^2. \quad (25)$$

Solving for the running of the mass parameter, we get

$$\partial_t M^2 = \frac{\partial_t \Gamma^{(2h)}(-M^2)}{Z_h(-M^2)}. \quad (26)$$

One of the goals of this work is to evaluate the phase diagram of quantum gravity and its fixed point structure. For this reason, it is convenient to derive β -functions for the dimensionless parameters. Then, the above equation translates into

$$\begin{aligned} \partial_t \mu &= -2\mu + \frac{\partial_t \Gamma^{(2h)}(-M^2)}{k^2 Z_h(-M^2)} \\ &=: \beta_\mu[\eta_h, \eta_c](g, \mu, \lambda^{(3)}, \lambda^{(4)}). \end{aligned} \quad (27)$$

The explicit form of the β -function is given in Appendix A. It is clear from (19) that the β -function for the running mass shows a functional dependence on the anomalous dimensions. It turns out that the final result for the β -function of μ and the momentum-dependent equation for the anomalous dimension $\eta(p)$ does not depend on the projection point, see Appendix B. The finite difference at $p^2 = -M^2$ is just the most convenient choice.

2. Integral equations for the anomalous dimensions

Starting from the general equation (18), using the above definition of the anomalous dimension and inserting (26), we obtain an integral equation for η_h which reads

$$\eta_h(p^2) = -\frac{\frac{\partial_t \Gamma^{(2h)}(p^2)}{Z_h(p^2)} - \frac{\partial_t \Gamma^{(2h)}(-M^2)}{Z_h(-M^2)}}{p^2 + M^2} [\eta_h, \eta_c]. \quad (28)$$

Note that all isolated Z -factors drop out, see (18). The same procedure can be applied for the ghost sector. Since there is no ghost mass, we trivially arrive from (20) at

$$\eta_c(p^2) = -\frac{\partial_t \Gamma^{(\bar{c}c)}}{p^2 Z_c(p^2)} [\eta_h, \eta_c]. \quad (29)$$

The explicit form of eqs. (28) and (29) is given in Appendix A. The full expressions of are derived and solved numerically, with the help of FORM [67], xTENSOR [68], and EIGEN [69].

C. The running gravitational coupling g

As already mentioned, we use geometrical flow equations for G_N in order to close the system of differential equations. This approach allows an inherently

diffeomorphism- invariant construction of flows in quantum gravity, see [70, 71]. It has been applied to the phase structure of quantum gravity in [2], where evolution equations β_g for the dynamical coupling g , and $\beta_{\bar{g}}$ for the background coupling \bar{g} are derived. In the present work we utilize the fact that the geometrical approach is directly related to the present approach in a flat background. In particular, the dynamical and background couplings in both approaches agree.

Moreover, with the fully momentum-dependent anomalous dimensions computed in the present work, we are able to directly incorporate effects of arbitrarily high powers of derivatives in the equations for $\beta_g, \beta_{\bar{g}}$ in [2]. The anomalous dimensions enter the geometric flow equations in very much the same way as in (18). However, the wave-function renormalizations in [2] are momentum-independent and can be pulled outside the integrals. This is not the case in our set-up. Entering the equations with the momentum-dependent $\eta_\phi(p^2)$ calculated via (28) leads to a modification on the level of the threshold functions Φ . These modified threshold functions are given in Appendix A.

With these ingredients, the general structure of the β -function for the dynamical gravitational coupling is given by

$$\beta_g[\eta_h, \eta_c](g, \mu) = 2g + F_g[\eta_h, \eta_c](g, \mu), \quad (30)$$

and the one for the background coupling takes the same form with g being replaced by \bar{g} and an individual loop contribution $F_{\bar{g}}[\eta_h, \eta_c](\bar{g}, \mu)$. The functionals F_g and $F_{\bar{g}}$ are given in Appendix A. Note that the flow equation of the background coupling depends on the dynamical coupling via the anomalous dimensions, while the converse does not hold.

D. The couplings $\Lambda^{(n)}$

In section III A we have introduced an approximation which takes into account scale-dependent couplings $\Lambda^{(n)}$ for the momentum-independent part of each vertex function. For the second order, we have identified $\Lambda^{(2)}$ as the graviton mass M^2 , see (16). In the present section we discuss the vertices with $n \geq 3$.

The Einstein-Hilbert truncation, which identifies all $\Lambda^{(n)}$ with the cosmological constant Λ , is ill-defined in the limit $\mu \rightarrow -1$. As we will see in section IV, this limit is approached by physical RG trajectories in the deep IR. This regime is crucial to understand the global phase structure of Euclidean quantum gravity: the couplings $\Lambda^{(n)}$ play a distinguished role, as the related singularities arise from the momentum-independent parts of the vertex functions. In order to cure the inconsistencies of the Einstein-Hilbert truncation, we deduce the singularity structure of the couplings $\Lambda^{(n)}$ with $n \geq 3$. The full details are given in Appendix C. Essentially, the idea is to expand the right-hand sides of the flow equations for the n -point functions in powers of $1 + \mu$ and taking

into account the singularities of highest order. Thus, for $\mu \rightarrow -1_+$ we use the ansatz

$$\lim_{\mu \rightarrow -1_+} \lambda^{(n)} \sim (1 + \mu)^{\alpha_n}, \quad (31)$$

for $n \geq 3$. We proceed by inserting this ansatz in the flow equations for $\Gamma^{(nh)}$ and analyze the generic loop integrals to leading order in the singularities that arise in the limits under consideration. Consistent scaling of both sides of the flow equations for arbitrary n leads to the relations

$$\alpha_n = \alpha_{n-2} + \alpha_4 - 1, \quad (32)$$

for $n \geq 5$ and

$$\alpha_4 \leq 2\alpha_3 - 1. \quad (33)$$

The parameter α_4 obeys the bound

$$\alpha_4 < 0. \quad (34)$$

The value of the parameters α_3 and α_4 cannot be obtained from the divergence analysis alone. They are dynamically determined by the flow of the three- and four-point function. This highlights again that the standard Einstein-Hilbert approximation with $\lambda^{(n)} = -\mu/2$ is inconsistent in the IR, and the non-existence of the IR fixed point cannot be inferred from such an approximation. It is also important to stress that the qualitative features of the phase diagram do not depend on the specific choice of α_3 and α_4 , see section IV A and Appendix D. In turn, the quantitative behaviour does only mildly depend on variations of these two parameters. Their flows will be studied in a forthcoming publication [66].

Still, we can estimate α_3 based on the saturation of the inequality (33). Moreover, the constant parts of the vertex functions are parametrically suppressed far away from the singular regime. This entails that there it is viable to identify $\Lambda^{(n)} = \Lambda^{(2)}$ as done in all other approximations used in the literature. From these conditions one obtains $\alpha_3 \approx -1/9$. More details are given in Appendix D. In Appendix E it is shown that

$$\lambda^{(n)} = -\frac{\mu}{2}(1 + \delta\lambda^{(n)}) \quad (35)$$

is consistent with all constraints, where $\delta\lambda^{(n)}$ parametrizes the deviation from the Einstein-Hilbert approximation. The latter is modeled by

$$\delta\lambda^{(n)} = \text{sgn}(\mu) \chi \left| \frac{\mu}{1 + \mu} \right|^{-\alpha_n}, \quad (36)$$

with χ a parameter to be tuned to match the aforementioned conditions.

E. The cosmological constant

It is left to discuss the role of the cosmological constant Λ in the present construction. Written on the right hand

side of the field equations, it can be interpreted as an additional source for gravity. In the classical limit, the quantum equations

$$\frac{\delta\Gamma}{\delta\phi} = J_{\text{ext}}, \quad (37)$$

with an external source J_{ext} , reduce to the classical equations of motion. Hence, it is natural to define the cosmological constant from the one-point function, i.e. we identify $\Lambda^{(1)} = \Lambda$ as the vacuum energy. More precisely, with the vertex construction (12), the one-point function takes the form

$$\left. \frac{\delta}{\delta h} \Gamma \right|_{g=\delta} \sim \frac{\Lambda}{\sqrt{G_N}} \sqrt{Z_h}. \quad (38)$$

Note that the one-point function does not enter the flow of higher order vertex functions. Consequently, the cosmological constant decouples from the β -functions for Newton's constant, the effective mass and the set of integral equations for the anomalous dimensions. On the other hand, these quantities obviously determine the running of the cosmological constant, i.e. the β -function for the dimensionless cosmological constant $\lambda := \Lambda/k^2$ is of the form

$$\begin{aligned} \dot{\lambda} &= \beta_\lambda[\eta_h, \eta_c](g, \lambda, \mu) \\ &= -2\lambda + g(A[\eta_h, \eta_c](\mu) + \lambda B[\eta_h, \eta_c](\mu)). \end{aligned} \quad (39)$$

The explicit form of this flow equation is given in Appendix A.

F. Regulators and stability

In order to test the quality of our truncation, we will use several regulators and vary the parameters χ and α_n introduced before. As regulators, on the one hand we use the class of exponential regulators given by

$$r_a(x) = \frac{1}{x(2e^{x^a} - 1)}, \quad (40)$$

where $x = p^2/k^2$ is the dimensionless squared momentum. In our analysis, we scanned the parameter range $a = \{2, 3, 4, 5, 6\}$. On the other hand, the Litim regulator, [72], is used,

$$r_{\text{opt}}(x) = \left(\frac{1}{x} - 1 \right) \theta(1 - x), \quad (41)$$

where $\theta(x)$ is the Heaviside step function. Note that this regulator is optimized within the leading order derivative expansion but not beyond, see [48, 72]. Also, with the semi-optimized regulator the divergence analysis for the $\Lambda^{(n)}$ is slightly different from the one performed in Appendix C, but leads to similar results.

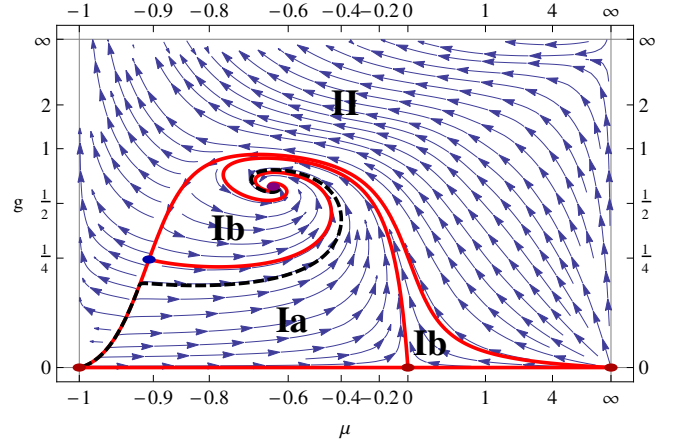


FIG. 2: Fixed points and global phase diagram in the (g, μ) -plane. Arrows point from the IR to the UV, red solid lines mark separatrices while dots indicate fixed points. The black dashed line is a specific trajectory that connects the UV fixed point with the non-trivial IR fixed point, which is analyzed further in the text. In analogy to [3], region Ia corresponds to trajectories leading to the massless IR fixed point, whereas region Ib leads to the massive IR fixed point. Region II is not connected to the UV fixed point, and thus physically irrelevant.

We also have scanned different values for the parameters χ and α_3 in (36), and we have restricted our investigation to the case of equality in (33). It turns out that the results do not depend on the specific choice of α_3 . Note that the parameter χ is bounded from above as otherwise the parametric suppression of the $\delta\lambda$ -contribution away from the singularity is lifted and the UV regime is changed. In Table VII in Appendix D, a table is given where the change of the UV fixed point values under a change of α_3 and χ can be ascertained.

IV. RESULTS

In this section we present our results. First, the global phase diagram is discussed. Subsequently, its UV and IR properties will be examined in more detail. In doing so, we will also make contact with older results. If not stated otherwise, all results and pictures are obtained with the specific choice of the exponential regulator r_4 .

A. The phase diagram

The phase diagram for the dynamical couplings (g, μ) is depicted in Figure 2. We find an attractive UV fixed point with coordinates

$$(g_*^{\text{UV}}, \mu_*^{\text{UV}}) = (0.614, -0.645), \quad (42)$$

and complex critical exponents $\theta_{1,2} = (-1.268 \pm 3.009i)$. This provides further non-trivial evidence for the asymp-

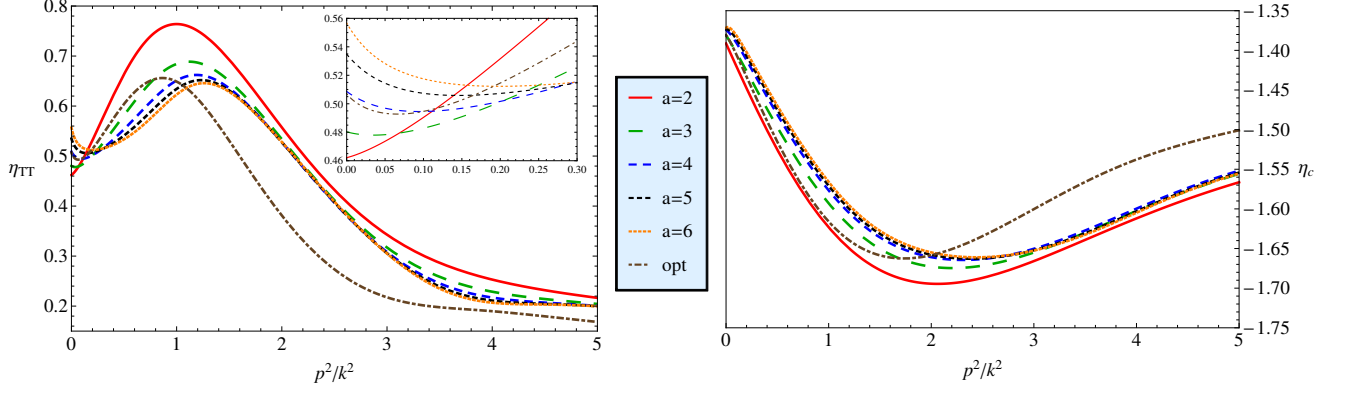


FIG. 3: The momentum-dependence of the anomalous dimensions of the graviton (left) and the ghost field (right) for different regulators at the respective UV fixed points. Only a weak dependence on the parameter is observed. The difference between optimized and exponential regulators is due to the fact that the modes are not integrated out at the same scale. From the fact that the quadratic external momentum terms cancel in the flow of the graviton [3], η_h goes to zero in the limit of large external momenta. The same is not true for the ghosts, where the anomalous dimension goes to a constant.

totically safe UV structure of quantum gravity. We also find the built-in repulsive Gaussian fixed point at $(g_*^{\text{Gauss}}, \mu_*^{\text{Gauss}}) = (0, 0)$, and a massive IR fixed point at $(g_*^{\text{IR}}, \mu_*^{\text{IR}}) = (0, \infty)$. The most striking feature of the present phase diagram is the confirmation of the attractive massless IR fixed point

$$(g_*^{\text{IR}}, \mu_*^{\text{IR}}) = (0, -1), \quad (43)$$

which was already found in [3], where it corresponds to a de-Sitter fixed point with $\lambda = 1/2$. This fixed point implies the global existence of trajectories connecting the UV fixed point with a finite IR fixed point. The present result is a clear confirmation that this IR fixed point is not a truncation artifact, but rather a physical property of the theory.

Importantly, it turns out to be an IR fixed point describing classical gravity. Physical initial conditions lead to globally defined trajectories that connect the non-trivial UV fixed point with the physical IR fixed point $(g_*^{\text{IR}}, \mu_*^{\text{IR}}) = (0, -1)$.

Note also that all UV-complete trajectories are also IR-complete, and end in either the massive or massless IR fixed point. In addition to this structure, there is a repulsive fixed point at $(g_*^{\text{rep}}, \mu_*^{\text{rep}}) = (0.250, -0.905)$. This fixed point was also found in [2]. All essential features do not depend on the choice of the regulator $r(x)$, and there are only minor quantitative changes induced by variations of the latter. The variation of the UV fixed point values under a variation of the vertex model parameters χ, α_3 , (36) is given in Table VII in Appendix C.

B. UV regime

Let us further investigate the properties of the UV fixed point. First of all, the existence of the fixed point does

a	2	3	4	5	6	opt
μ_*	-0.637	-0.641	-0.645	-0.649	-0.651	-0.489
g_*	0.621	0.622	0.614	0.606	0.600	0.831
\bar{g}_*	0.574	0.573	0.567	0.559	0.553	0.763
λ_*	0.319	0.316	0.316	0.318	0.319	0.248
EVs	-1.284	-1.284	-1.268	-1.255	-1.244	-1.876
	$\pm 3.247i$	$\pm 3.076i$	$\pm 3.009i$	$\pm 2.986i$	$\pm 2.974i$	$\pm 2.971i$
	-2	-2	-2	-2	-2	-2
	-1.358	-1.360	-1.360	-1.358	-1.356	-1.370

TABLE I: UV fixed point values and eigenvalues for different regulator parameters a , and the optimized regulator, with parameter values $\alpha_3 = -0.1$ and $\chi = 0.1$.

	here	[5]	[3]	[2]	[73]	[65]	Table VI
\bar{g}_*	0.763	1.178	2.03	0.966	1.055	1.617	1.684
λ_*	0.248	0.250	0.22	0.132	0.222	-0.062	-0.035
$\bar{g}_* \lambda_*$	0.189	0.295	0.45	0.128	0.234	-0.100	-0.059

TABLE II: Comparison of the UV fixed point coordinates with earlier results for the optimized cutoff. Parameter values are $\alpha_3 = -0.1$ and $\chi = 0.1$. Methods of the references (in order): background approximation [5], bi-local projection [3], geometric approach [2], bi-metric approach [73]. The mixed approach is applied in [65] and is also discussed in the present paper in the last paragraph of this subsection, Table VI.

not depend on the specific choice of the regulator. Moreover, it is attractive in all four directions investigated here. Furthermore, even though the critical exponents of the dynamical quantities (g, μ) are complex, the ones of the physical background couplings (\bar{g}, λ) are real. This was also found in [3] and [65]. Notice that the eigenvalue corresponding to \bar{g} is exactly -2, which can be immediately inferred from the specific structure of the background coupling flow equation. Also, the eigenvalue cor-

responding to λ is inherently real, as its flow equation is a polynomial of order one in the cosmological constant. All these points are summarized in [Table I](#).

The connection to earlier results is drawn in [Table II](#). The present results support the qualitative reliability of the Einstein-Hilbert type approximations in the UV regime.

The couplings as functions of the RG scale k along one selected trajectory (marked as a dashed black line in the phase diagram) are shown in [Figure 5](#). One can see how the couplings tend to their finite fixed point values in the UV. The IR regime will be discussed below.

A further quantity of interest is the anomalous dimension. The momentum-dependence of both graviton and ghost anomalous dimension is given in [Figure 3](#) for all used regulators at their respective UV fixed point. As one can see, only quantitative differences occur. The graviton anomalous dimension is of the order of 0.5, whereas the ghost anomalous dimension is of the order of -1.5 . The difference between exponential and optimized regulators is due to the fact that the regulators integrate out modes at different scales. Consequently, the effective cut-off scale is regulator-dependent. A formal discussion of scale-optimization can be found in [\[48\]](#), and is applied in the context of finite temperature Yang-Mills theory in [\[74\]](#). For instance, for the exponential cutoff $r_a(x)$ with $a = 4$, we find that if one rescales

$$k_{\text{opt}} \rightarrow 1.15 k_{\text{opt}}, \quad (44)$$

the momentum-dependence of the anomalous dimension with a optimized regulator matches the one obtained with an exponential regulator, see [Figure 4](#). In general, we observed that the (TT-part of the) graviton anomalous dimension is positive, however there are indications that this does not remain so when the other degrees of freedom of the graviton receive an individual anomalous dimension [\[66\]](#). On the other hand, the ghost anomalous dimension is strictly negative, as was already found in [\[75\]](#) and [\[76\]](#). We also note that the anomalous dimensions are not the leading contribution to the flow. This means that by setting $\eta(q^2) = 0$ on the RHS of the flow [\(19\)](#), one captures all qualitative properties discussed here. Hence, the anomalous dimensions only constitute correction effects while the leading term on the RHS of the flow equations is the one proportional to \dot{r} . In the ghost sector this pattern is even more pronounced, and dynamical ghost effects on the phase diagram and the running couplings are very small.

Derivative expansion: We close this section with a discussion of the stability of the (covariant) derivative expansion which is the standard approximation scheme used so far. The first calculation of the graviton anomalous dimension has been presented in [\[3\]](#) within the FRG. There, the flow is projected at $p = k$. In the work [\[65\]](#) a derivative expansion around $p = 0$ is performed. The full results in the present study show a strong momentum dependence of the correlation functions as well as

a	2	3	4	5	6	opt
η_{der}	0.46	0.48	0.51	0.54	0.56	0.51

TABLE III: Anomalous dimension η_{der} in the lowest order derivative expansion derived from the full flow.

a	2	3	4	5	6	opt
η_{der}	0.44	0.50	0.58	0.66	0.74	0.61

TABLE IV: Full anomalous dimension η_{der} in the lowest order derivative expansion derived from the full flow.

their flows in the cut-off regime with $p^2/k^2 \lesssim 1$. Such a strong momentum dependence of the flows either requires higher orders in the derivatives or a non-local expansion that works-in the information of momenta close to zero and those close to $p^2/k^2 = 1$, see [\[3, 74, 77\]](#).

Note that there is a strong cut-off dependence of the graviton anomalous dimension at the UV fixed point for small momenta $p^2/k^2 \lesssim 0.05$, see [Figure 3](#). The occurrence of this regime is presumably related to the mass-scale set by the fixed point value of μ . Here we investigate its impact on the value of η_h in the leading order of the derivative expansion. We also consider a variation of the expansion point. We also use the present results with full momentum-dependence in order to investigate the reliability of the derivative expansion. There, the computation of the anomalous dimension requires

$$\frac{\partial_{p^2} \dot{\Gamma}_k^{(2h)}}{Z} = -\eta + \frac{\dot{Z}'}{Z}(x + \mu) + \frac{Z'}{Z}(2\mu + \dot{\mu}), \quad (45)$$

e.g. at vanishing momentum, $x = p^2/k^2 = 0$. On the other hand, the momentum derivative of η gives the relation

$$\frac{\dot{Z}'}{Z} = -\eta' - \frac{Z'}{Z}\eta. \quad (46)$$

Inserting [\(46\)](#) in [\(45\)](#) leads to

$$\frac{\partial_{p^2} \dot{\Gamma}_k^{(2h)}}{Z} = -\eta - \eta'(x + \mu) + \frac{Z'}{Z}[(2 - \eta)\mu - \eta x + \dot{\mu}]. \quad (47)$$

In the lowest order derivative expansion, that is $\Gamma_k^{(2h)} = Z_k(p^2 + m^2)$, the anomalous dimension η_{der} is given by (minus) [\(47\)](#) evaluated at $x = 0$. Moreover, the lowest order implies $Z' = 0$ and we simply arrive at

$$\eta_{\text{der}} = \eta(0). \quad (48)$$

For the regulators used in the present work this leads to anomalous dimensions listed in [Table III](#). However, the full lowest order derivative expansion takes into account the Z' -terms on the right hand side. At vanishing momentum there is the relation

$$\left. \frac{Z'}{Z} \right|_{x=0} = \frac{1}{2} \eta' \Big|_{x=0}. \quad (49)$$

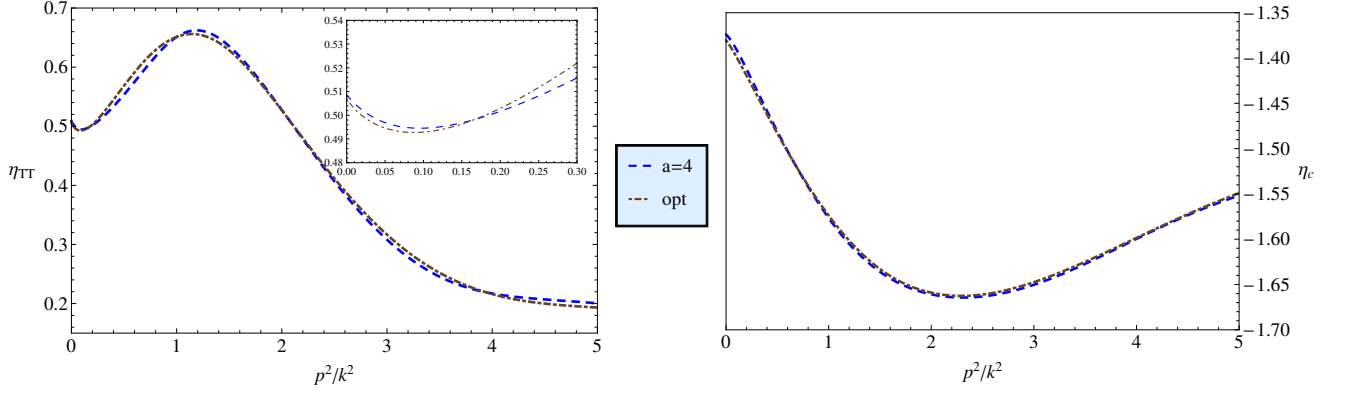


FIG. 4: Comparison of the momentum dependence of the graviton and the ghost anomalous dimension with the exponential regulator with $a = 4$ on the one hand, and the optimized regulator with the cutoff-rescaling (44) on the other.

α	0	0.25	0.5	0.75	1	1.15
η_{der}	0.57	0.50	0.39	0.25	0.074	-0.016

TABLE V: Anomalous dimension η_{der} in the standard derivative expansion with optimized regulator in an expansion around $p = \alpha k$ with $(\mu = 0, g = 1)$.

This is easily derived from

$$Z_k(p^2) = Z_{k_0}(p^2) \exp \left\{ - \int_{k_0}^k \frac{d\bar{k}}{\bar{k}} \eta_{\bar{k}}(p^2) \right\}, \quad (50)$$

where both k and k_0 are in the scaling regime. The latter condition implies that $Z'/Z = Z'_k/Z_k(0)$ and $\eta' = \eta'_k(0)$ are independent of $\bar{k} \in [k_0, k]$. Then we conclude that at $x = 0$ we have

$$\frac{Z'_k}{Z_k} = \frac{Z'}{Z} \frac{k^2}{k_0^2} + \frac{1}{2} \eta' \left(1 - \frac{k^2}{k_0^2} \right), \quad (51)$$

for all k, k_0 in the scaling regime and we are led to (49). Hence, in the scaling regime (with $\dot{\mu} = 0$) the full anomalous dimension in the derivative expansion at $x = 0$ is given by

$$\eta_{\text{der}} = \eta \left(1 + \frac{1}{2} \eta' \mu \right), \quad (52)$$

leading to Table IV. These results seem to be much more stable than the approximation (48).

To complete the present reliability analysis of Taylor expansions in momenta p^2 , we also investigate expansions about a general expansion point $p = \alpha k$. We present results for the optimized regulator and evaluate the anomalous dimension for $g = 1, \mu = 0, \eta_c = 0$. The conclusions of this study do not depend on the choice of these parameters. As one can see, the anomalous dimension of the graviton in a derivative expansion strongly depends on the specification parameter α . This

relates to the fact that such an expansion only works well if the full flow of the propagator shows a mild momentum dependence. This is not the case for the flow of the graviton two-point function, see [3]. In general, even the sign of the anomalous dimension depends on the specification parameter. We conclude that a derivative expansion in quantum gravity with $\alpha = 0$ has to be used with great caution.

Effect of identifications of couplings in the UV: As already mentioned, the present approximation is the first work that employs individual running couplings for the momentum-independent part of each vertex function. In particular, the graviton mass term should not be identified with the cosmological constant. Still, we have shown, that the full expansion with momentum-dependent wave function renormalizations and a mass term for the fluctuating graviton h provides UV fixed point results in qualitative agreement with that of the standard background field approach, if we identify the mass a posteriori with (minus 1/2 of) the cosmological constant. Within such an identification we have a deSitter fixed point.

For completeness, we also have investigated a mixed approach: We use a flat anomalous dimension η_h in a derivative expansion about vanishing momentum, or a momentum-dependent one, $\eta_h(p^2)$, for the fluctuating graviton. In turn, the flows of the graviton mass and the Newton coupling g are extracted from the flow of the cosmological constant and the Newton coupling in the background field approximation. This can be interpreted as an intermediate step towards the full approximation studied here. Interestingly this leads to a very small and negative fixed point value for the cosmological constant, see also [65] for such a mixed expansion with a flat anomalous dimension. Our fixed point results for the case with a flat anomalous dimension are given in Table VI. They are in qualitative agreement with the results of [65]. Notably, the results in the mixed approach deviate from both, the background field results and that of the full approximation introduced in the present work.

a	2	3	4	5	6	opt
g_*	1.68	1.72	1.75	1.77	1.80	1.68
λ_*	-0.064	-0.076	-0.088	-0.100	-0.110	-0.035
η_h^{der}	0.81	0.93	1.03	1.14	1.24	0.86
η_c^{der}	-1.08	-1.05	-1.04	-1.03	-1.01	-0.75

TABLE VI: Fixed point values g_* and λ_* and anomalous dimension η_{der} at this fixed point in the mixed approach.

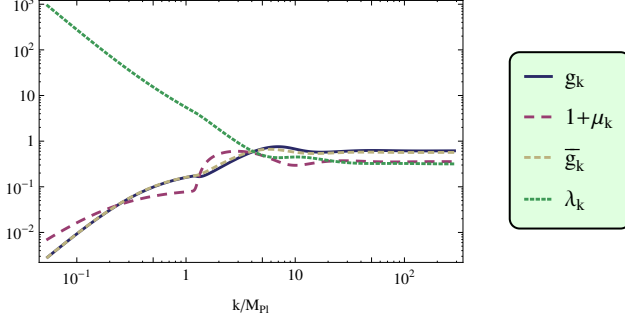


FIG. 5: The running couplings as functions of the renormalization scale k in units of the Planck mass. In the UV the couplings tend to their finite fixed point values. As one follows the trajectories down to the IR, one can see the scaling behaviour in the vicinity of the IR fixed point.

We have also checked that this originates in the identification of the mass term with the cosmological constant, the given alternative choices for the flow of the Newton constant do not alter this result.

C. IR regime

The non-trivial IR fixed point is located at $(g, \mu) = (0, -1)$. The most important feature is that it is a classical one, i.e. the essential couplings scale classically and all quantum contributions vanish: The gravitational couplings and the cosmological constant scale as

$$g, \bar{g} \sim k^2, \quad \lambda \sim k^{-2}, \quad (53)$$

and the anomalous dimensions vanish,

$$\eta_h \rightarrow 0, \quad \eta_c \rightarrow 0, \quad (54)$$

see Appendix F. This leads to flow trajectories that connect the asymptotically safe UV regime for $k \rightarrow \infty$ and short distances, with a classical IR regime for $k \rightarrow 0$ and large distances. Since μ approaches a finite value in the limit $k \rightarrow 0$, the dimensionful mass $M^2 = \mu k^2$ vanishes in the deep IR. Accordingly, this fixed point corresponds to a massless theory on large distances, which is consistent with gravity as a force with infinite range. Moreover, the scaling of Newton's coupling (53) allows us to identify

a scale in the following way. As g (or \bar{g}) scales classically, the coefficient of proportionality, say C , is nothing else than the Newton constant, because

$$G_N = gk^{-2} = Ck^2k^{-2} = C. \quad (55)$$

Thus, scales are measured in units of the Planck mass, $M_{\text{Pl}}^2 = 1/C$. The physical trajectory is then fixed by measuring the relevant couplings, that is the (background) Newton constant and cosmological constant, at a given scale. In Figure 5 one can see both, the classical scaling in the IR as well as the vanishing of the β -functions in the vicinity of the UV fixed point for large k . The classical scaling regime extends roughly up to one order of magnitude below the Planck scale. This implies the absence of quantum gravity effects for energies $E \ll M_{\text{Pl}}$, as it is expected in a theory without a large volume compactification of extra-dimensions. Note also that the difference between the two couplings g and \bar{g} is hardly visible, which justifies to some extent the background approximation for the Newton constant.

V. SUMMARY AND OUTLOOK

We have presented a quantum gravity calculation that shows a classical regime on large distances, and asymptotically safe physics in the non-perturbative UV limit. The behaviour at large distances relates to an attractive IR fixed point with classical scaling behaviour. This implies that the dimensionful Newton constant G_N and the cosmological constant Λ do not depend on the energy scale (inverse length scale) for large distances. Hence, for the first time, this includes the domain of classical gravity, that has been tested experimentally, in the renormalization group approach to quantum gravity. The classical gravity regime in the vicinity of the IR fixed point is connected to a non-perturbative UV fixed point, which ensures the finiteness of scattering amplitudes at arbitrary high energies. The small dependence of the results on the regulator indicates stability of the present truncation. Technically, this work introduces a novel approximation scheme in RG-gravity calculations. This scheme has two essential features: First, we work in a vertex expansion with fully momentum-dependent wave-function renormalizations for the graviton and for the ghost field. Second, the higher order correlation functions are parametrized by additional couplings for their momentum-dependent and momentum-independent parts. The latter become important in the IR and their properties are determined by a self-consistency scaling analysis. In particular, we show that the momentum-independent part of the two point function cannot be identified with the cosmological constant at large distances.

In summary, this work provides further evidence for the asymptotic safety scenario in quantum gravity. In addition it substantiates the physics at the IR fixed point

found in [2, 3]. By now, the approximation is quantitative enough to produce classical scaling for the couplings G_N and Λ for large length scales, in accordance with experimental observations. The present approximation is readily extended to include higher correlation functions which will be reported on in future work [66].

Acknowledgments

We thank Tobias Henz, Daniel F. Litim and Christof Wetterich for discussions and collaboration on related subjects. We thank Alessandro Codello for providing us with an updated version of [65] prior to substitution on arXiv. JMP thanks the Yukawa Institute for Theoretical Physics, Kyoto University, where this work was completed during the YITP-T-13-05 on 'New Frontiers in QCD'. This work is supported by Helmholtz Alliance HA216/EMMI and by ERC-AdG-290623.

Appendix A: Flow equations

The modified threshold functions introduced in [section III C](#) are given by:

$$\Phi_n^p[\eta](\omega) = \frac{1}{\Gamma(n)} \int_0^\infty dx x^n \frac{\dot{r}(x) - \eta(x)r(x)}{(x(1+r(x)) + \omega)^p}. \quad (\text{A1})$$

With these threshold functions, the geometric flow equations in [2], improved by momentum-dependent anomalous dimensions, are given by

$$\dot{\bar{g}} = 2\bar{g} - \frac{\bar{g}^2}{2\pi} \left[\frac{2}{3} \Phi_1^1[\eta_h](\mu) + \frac{10}{3} \Phi_2^2[\eta_h](\mu) + \frac{5}{12} \Phi_1^1[\eta_c](0) + \frac{5}{4} \Phi_2^2[\eta_c](0) \right], \quad (\text{A2})$$

$$\dot{g} = 2g - \frac{g^2}{2\pi} \left[\frac{2}{3} \Phi_1^1[\eta_h](\mu) + \frac{10}{3} \Phi_2^2[\eta_h](\mu) + \frac{5}{24} \Phi_1^1[\eta_c](0) + \frac{5}{8} \Phi_2^2[\eta_c](0) + \dot{\mu} \left(\frac{2}{3} \Phi_1^2[0](\mu) + \frac{20}{3} \Phi_2^3[0](\mu) \right) \right]. \quad (\text{A3})$$

The flows of the two-point functions are given by

$$\frac{\partial_t \Gamma^{(2h)}(p^2)}{Z_h(p^2)} = g \int_0^\infty dq \int_{-1}^1 dx \sqrt{1-x^2} \frac{q^3}{3\pi^2} \times \left[- \frac{f_c(p, q, x)(\dot{r}_1 - \eta_c(q^2)r_1)}{(1+r_1)^2(1+r_2)} \right] \quad (\text{A4})$$

$$\begin{aligned} & - \frac{6q^2(3p^2 + 6q^2 - 8\lambda^{(4)})(\dot{r}_1 - \eta_h(q^2)r_1)}{(q^2(1+r_1) + \mu)^2} \\ & + \frac{f_h(p, q, x, \lambda^{(3)})(\dot{r}_1 - \eta_h(q^2)r_1)}{(q^2(1+r_1) + \mu)^2((p^2 + 2pqx + q^2)(1+r_2) + \mu)} \Big], \\ & \frac{\partial_t \Gamma^{(\bar{c}c)}(p^2)}{Z_c(p^2)} = -g \int_0^\infty dq \int_{-1}^1 dx \sqrt{1-x^2} \frac{4q^3}{3\pi^2} \times \\ & \frac{p^2(3+6x^2) + pqx(-2+20x^2) + q^2(5-12x^2+16x^4)}{p^2 + 2pqx + q^2} \times \\ & \left[\frac{\dot{r}_1 - \eta_c(q^2)r_1}{(1+r_1)^2((p^2 + 2pqx + q^2)(1+r_2) + \mu)} + \frac{q^2(\dot{r}_1 - \eta_h(q^2)r_1)}{(q^2(1+r_1) + \mu)^2(1+r_2)} \right]. \end{aligned} \quad (\text{A5})$$

Here, we have introduced the short cuts $r_1 = r(q^2)$ and $r_2 = r(p^2 + 2pqx + q^2)$. The functions $f_c(p, q, x)$ and $f_h(p, q, x, \lambda^{(3)})$ read

$$f_c(p, q, x) = \frac{16(p^2(2+x^2) + 6pqx + 3q^2)}{p^2 + 2pqx + q^2} \quad (\text{A6})$$

and

$$\begin{aligned} f_h(p, q, x, \lambda^{(3)}) &= \frac{4q^2}{5(p^2 + 2pqx + q^2)} \times \\ & \left(15p^6(1+2x^2) + 10p^5qx(7+8x^2) \right. \\ & + p^4q^2(21+208x^2+56x^4) + 140p^3q^3x(1+2x^2) \\ & + 4p^2q^4(7+76x^2+22x^4) \\ & + 8pq^5x(17+11x^2+2x^4) \\ & + 4q^6(7+6x^2+2x^4) - 4\lambda^{(3)}[15p^4(1+4x^2) \\ & + 30p^3qx(3+4x^2) + p^2q^2(-9+248x^2+16x^4) \\ & + 20pq^3x(5+4x^2) + 20q^4(1+2x^2)] \\ & + 8(\lambda^{(3)})^2[15p^2(1+x^2) + 20pqx(2+x^2) \\ & \left. + 2q^2(9+2x^2+4x^4)] \right). \end{aligned} \quad (\text{A7})$$

Finally, the flow equation for λ from the one-point function is given by

$$\dot{\lambda} = -2\lambda + g \left[\int_0^\infty dq \frac{3q^7(1+2\lambda^{(3)})}{4\pi} \frac{\dot{r}(q^2) - \eta_h(q^2)r(q^2)}{(q^2(1+r(q^2)) + \mu)^2} \right]$$

$$+ \int_0^\infty dq \frac{q^3(3 - \lambda^{(3)})}{3\pi} \frac{\dot{r}(q^2) - \eta_c(q^2)r(q^2)}{(1 + r(q^2))^2} \Big]. \quad (\text{A8})$$

Appendix B: Projection procedure

Here, we want to argue why the projection procedure to obtain the flow equation for the mass and the integral equation for the graviton anomalous dimension is the physical one. First the anomalous dimension must be finite everywhere, in particular at the pole. Otherwise, the wave-function renormalization could be written as

$$Z_h(p^2) = (p^2 + \mu)^\omega \tilde{Z}_h(p^2) \quad (\text{B1})$$

with a nonzero parameter ω and $Z_h(-\mu)$ finite and nonzero. However, the wave-function renormalization should only determine the residue at the propagator pole. Thus, we assume that the anomalous dimension is finite.

Next, we consider the flow equation of the two-point function,

$$- \eta_h(p^2)(p^2 + \mu) + \dot{\mu} + 2\mu = \frac{\partial_t \Gamma^{(2h)}(p^2)}{Z_h(p^2)}. \quad (\text{B2})$$

We can evaluate this equation at an arbitrarily chosen fixed momentum, say ℓ , to obtain the β -function of the mass:

$$\dot{\mu} = -2\mu + \frac{\partial_t \Gamma^{(2h)}(\ell^2)}{Z_h(\ell^2)} + \eta_h(\ell^2)(\ell^2 + \mu). \quad (\text{B3})$$

Subtracting this from the original equation leaves an integral equation for the anomalous dimension,

$$\eta_h(p^2) = - \frac{\frac{\partial_t \Gamma^{(2h)}(p^2)}{Z_h(p^2)} - \frac{\partial_t \Gamma^{(2h)}(\ell^2)}{Z_h(\ell^2)}}{p^2 + \mu} + \eta_h(\ell^2) \frac{\ell^2 + \mu}{p^2 + \mu}. \quad (\text{B4})$$

One easily sees that the right hand side of this equation diverges at $p^2 = -\mu$, if $\eta(\ell^2)$ is not chosen appropriately. As we already know that the anomalous dimension must be finite everywhere, we conclude that

$$\eta_h(\ell^2) = \frac{\frac{\partial_t \Gamma^{(2h)}(-\mu)}{Z_h(-\mu)} - \frac{\partial_t \Gamma^{(2h)}(\ell^2)}{Z_h(\ell^2)}}{\ell^2 + \mu}. \quad (\text{B5})$$

This can be reinserted into (B4), leading to

$$\eta_h(p^2) = - \frac{\frac{\partial_t \Gamma^{(2h)}(p^2)}{Z_h(p^2)} - \frac{\partial_t \Gamma^{(2h)}(-\mu)}{Z_h(-\mu)}}{p^2 + \mu}, \quad (\text{B6})$$

which is the equation originally proposed in the main text. We can use the expression for $\eta_h(\ell^2)$ also for the flow equation of the mass, resulting in

$$\dot{\mu} = -2\mu + \frac{\partial_t \Gamma^{(2h)}(-\mu)}{Z_h(-\mu)}, \quad (\text{B7})$$

again reproducing the result from the main text. Thereby, we have shown, under the reasonable condition of a finite anomalous dimension, that our flow equations are unique.

Appendix C: Infrared scaling analysis

Here, we discuss the IR divergence analysis in more detail. Before we can proof a recursion relation for the parameters α_n , we discuss some general properties of such a setting.

Prerequisites: The flow of a general n -point vertex function includes generic loop integrals with dimensionless external momenta p_i and loop momentum q of the form

$$\int \frac{d^4 q}{(2\pi)^4} \frac{f_n(q, p_i)}{(q^2(1 + r(q^2)) + \mu)^2} \times \prod_{i=1}^{n-2} ((p_i + q)^2(1 + r((q + p_i)^2)) + \mu)^{-1}, \quad (\text{C1})$$

with a function $f_n(q, p_i)$ resulting from contractions of the tensor structure \tilde{T} defined in (14). Obviously, the divergences are strongest at vanishing external momenta $p_i = 0$. In this case, all internal propagators carry the loop momentum q and we are left with

$$\int \frac{d^4 q}{(2\pi)^4} \frac{f_n(q, p_i = 0)}{(q^2(1 + r(q^2)) + \mu)^n}. \quad (\text{C2})$$

Moreover, in the limit $\mu \rightarrow -1$, these divergences emerge from small momentum modes near $q = 0$. Consistent regulators need to fulfill

$$\lim_{x \rightarrow 0} x(1 + r(x)) = 1 + \zeta x + \mathcal{O}(x^2) \quad (\text{C3})$$

with $\zeta > 0$, because otherwise, the denominator in (C2) exhibits a zero for $\mu > -1$. The highest pole order is contained in the momentum-independent part $f_n^0 := f_n(q = 0, p_i = 0)$. Neglecting the angular integration, and by the above reasoning, the most divergent part of the integral takes the form

$$\int_0^{\delta > 0} dq \frac{q^3 f_n^0}{(q^2 + \epsilon)^n}, \quad (\text{C4})$$

where we introduced $\epsilon = 1 + \mu$ for convenience. These expressions can be integrated which leads to a divergence structure of the form

$$\int_0^{\delta > 0} dq \frac{q^3}{(q^2 + \epsilon)^n} \sim \begin{cases} \text{finite} & \text{if } n < 2 \\ \log \epsilon & \text{if } n = 2 \\ \epsilon^{2-n} & \text{if } n > 2 \end{cases}. \quad (\text{C5})$$

In a simple Einstein Hilbert truncation one identifies the constant, momentum-independent parts of the n -point vertex functions $\lambda^{(n)}$ with the mass term (or with the cosmological constant), i. e. $\lambda^{(n)} = -\mu/2$ for all n . However, this approximation incorporates a scaling inconsistency, as we will see by the divergence analysis below.

The following analysis is based on a matching of terms in the limit $\epsilon \rightarrow 0$ on the RHS and the LHS of the flow

equations for n -point vertex functions. As a generalization of the Einstein-Hilbert construction we allow for a power law behaviour in ϵ in the limit under consideration. In such an expansion, logarithmic contributions are sub-leading, do not change the power law and are therefore discarded. Moreover, we keep only the leading order terms, i.e. we assume a power law

$$\lambda^{(n)} \stackrel{\epsilon \rightarrow 0}{\sim} \epsilon^{\alpha_n}, \quad n \geq 3, \quad (\text{C6})$$

and suppress terms of the form $\epsilon^{\tilde{\alpha}_n}$ with $\tilde{\alpha}_n > \alpha_n$, since we are interested in the limit $\epsilon \rightarrow 0$. Moreover, we observe that the ϵ -dependence of the function f_n^0 is completely stored in the parameters $\lambda^{(n)}$. Accordingly, these are the only terms that we have to take into account in an ϵ -scaling analysis. The generic form of a β -function for $\lambda^{(n)}$ is of the form

$$\dot{\lambda}^{(n)} = -2\lambda^{(n)} + g (\text{loop} - \text{terms}), \quad (\text{C7})$$

i.e. a canonical term and loop contributions which are always proportional to the gravitational coupling g . First, we show that the canonical term does not dominate the β -functions for $\lambda^{(n)}$ with $n = 2, 3, 4$ in the limit $\epsilon \rightarrow 0$. In order to do so, we assume that the canonical term in the beta functions for $\lambda^{(3)}$ dominates in the limit $\epsilon \rightarrow 0$, i.e. $\dot{\lambda}^{(3)} \stackrel{\epsilon \rightarrow 0}{\sim} -2\lambda^{(3)}$, which implies $\lambda^{(3)} \stackrel{\epsilon \rightarrow 0}{\sim} 1/k^2$. On the other hand, dominance of the canonical term means $\dot{\lambda}^{(3)} \stackrel{\epsilon \rightarrow 0}{\sim} \epsilon^{\alpha_3}$. From Figure 6 and (C5) we can see that there is a diagram producing a term $\stackrel{\epsilon \rightarrow 0}{\sim} \epsilon^{3\alpha_3-2}$. Dominance of the canonical term then implies $\alpha_3 > 1$. In this case $\lambda^{(3)} \stackrel{\epsilon \rightarrow 0}{\sim} 0$. This contradicts $\lambda^{(3)} \stackrel{\epsilon \rightarrow 0}{\sim} 1/k^2$ as long as there is no UV fixed point at $\epsilon = 0$. The same argument goes through for $\lambda^{(4)}$ by using the term $\stackrel{\epsilon \rightarrow 0}{\sim} \epsilon^{2\alpha_4-1}$ on the RHS of the respective flow equation. Thus, we know that the canonical term is sub-leading or of equal order as the loop terms. With a case-by-case analysis of $(\lambda_3 \leq 1, \lambda_4 \leq 1)$, one can show that $\alpha_4 < 1$. Then, using (C13) below it can be deduced that the canonical term in the flow equation for λ^4 is indeed subleading and $\dot{\lambda}^4 \stackrel{\epsilon \rightarrow 0}{\sim} g$. Together with (C15) this in turn implies that $\dot{\epsilon} \stackrel{\epsilon \rightarrow 0}{\sim} g$ and therefore, the canonical term in $\dot{\epsilon}$ is irrelevant as well. Accordingly either

$$\alpha_4 < 0 \quad \text{or} \quad \alpha_3 < 1/2, \quad (\text{C8})$$

and additionally, the canonical term in $\dot{\lambda}^n$ for all n is subleading too, as both sides of the respective flow equation must be proportional to g .

Lemma 1: *Assuming the results in Prerequisites, in particular a power law*

$$\lambda^{(n)} \stackrel{\epsilon \rightarrow 0}{\sim} \epsilon^{\alpha_n}, \quad (\text{C9})$$

with $n \geq 3$, the hierarchy of flow equations implies

$$\alpha_4 \leq 2\alpha_3 - 1. \quad (\text{C10})$$

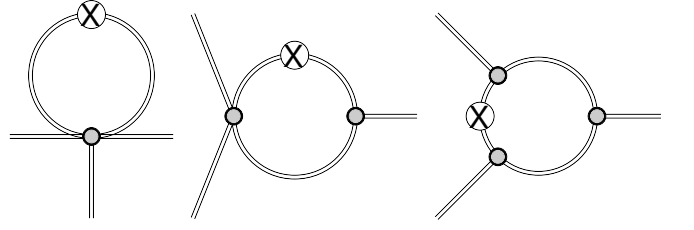


FIG. 6: Diagrams contributing to the divergence analysis of the three-point function of the graviton.

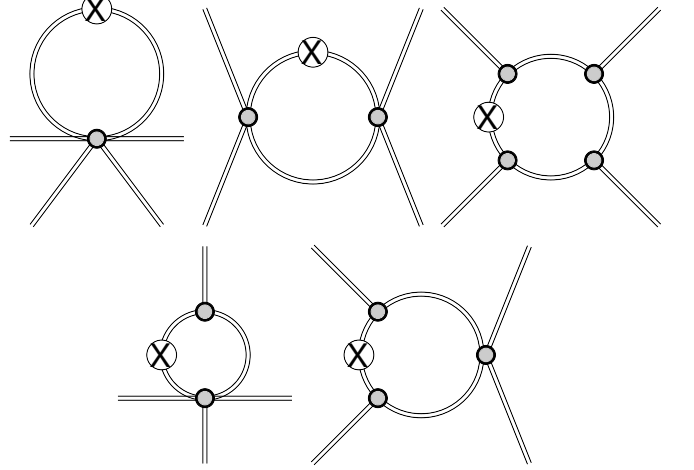


FIG. 7: Diagrams contributing to the divergence analysis of the four-point function of the graviton.

Proof: The flow of the two point function (evaluated at vanishing external momentum) leads to the relation

$$\begin{aligned} \dot{\mu} &= \dot{\epsilon} \stackrel{\epsilon \rightarrow 0}{\sim} g \max \left\{ \left| \lambda^{(4)} \right|, \frac{(\lambda^{(3)})^2}{\epsilon} \right\} \\ &\sim g \max \{ \epsilon^{\alpha_4}, \epsilon^{2\alpha_3-1} \}, \end{aligned} \quad (\text{C11})$$

where the terms in the curly brackets $\{\cdot, \cdot, \dots\}$ indicate the leading contributions arising from the distinct diagrams. The diagrams generating the running of the three point function (see Figure 6) lead to

$$\dot{\lambda}^{(3)} \stackrel{\epsilon \rightarrow 0}{\sim} g \max \{ \epsilon^{\alpha_5}, \epsilon^{\alpha_3+\alpha_4-1}, \epsilon^{3\alpha_3-2} \}. \quad (\text{C12})$$

The next order in the hierarchy, the flow equation for $\Gamma^{(4h)}$, has the diagrammatic representation Figure 7. This means that the diagrams scale in the limit $\epsilon \rightarrow 0$ as

$$\begin{aligned} \dot{\lambda}^{(4)} &\stackrel{\epsilon \rightarrow 0}{\sim} g \max \{ \epsilon^{4\alpha_3-3}, \epsilon^{2\alpha_3+\alpha_4-2}, \\ &\quad \epsilon^{2\alpha_4-1}, \epsilon^{\alpha_3+\alpha_5-1}, \epsilon^{\alpha_6} \}. \end{aligned} \quad (\text{C13})$$

On the other hand, we can calculate $\dot{\lambda}^{(3)}$ and $\dot{\lambda}^{(4)}$ from (C9), i.e. the LHS of the flow equation. Using (C11), this yields

$$\dot{\lambda}^{(3)} \stackrel{\epsilon \rightarrow 0}{\sim} \epsilon^{\alpha_3-1} \dot{\epsilon} \stackrel{\epsilon \rightarrow 0}{\sim} g \max \{ \epsilon^{\alpha_3+\alpha_4-1}, \epsilon^{3\alpha_3-2} \}, \quad (\text{C14})$$

and

$$\dot{\lambda}^{(4)} \stackrel{\epsilon \rightarrow 0}{\sim} \epsilon^{\alpha_4-1} \dot{\epsilon} \stackrel{\epsilon \rightarrow 0}{\sim} g \max \{ \epsilon^{2\alpha_4-1}, \epsilon^{\alpha_4+2\alpha_3-2} \}. \quad (\text{C15})$$

Consistency requires matching of the leading terms on both sides of the flow equations.

If the leading term on the LHS is known, the matching condition induces inequalities on the RHS and we can obtain relations for α_n .

On the left hand sides of the flow equations for the three- and the four-point functions we have in each case two terms, (C14) and (C15). Let us now study the different cases for the leading terms. Considering the three-point function, the different cases can be written as

$$\alpha_3 + \alpha_4 - 1 \begin{matrix} \leq \\ \geq \end{matrix} 3\alpha_3 - 2. \quad (\text{C16})$$

Analogously, from the LHS of the four-point function we obtain one of the “dual” relations

$$2\alpha_4 - 1 \begin{matrix} \leq \\ \geq \end{matrix} \alpha_4 + 2\alpha_3 - 2. \quad (\text{C17})$$

Obviously, the above relations (C16) and (C17) are equivalent, i.e. if one of the relations $>, =, <$ is true, the corresponding relation holds for the other expression. Consequently, if we know the leading term on the LHS of the flow equation for $\Gamma^{(3h)}$, we know the leading term in the corresponding equation for $\Gamma^{(4h)}$ and vice versa. We proceed with a case-by-case analysis.

(i) *Assume*

$$\alpha_3 + \alpha_4 - 1 \geq 3\alpha_3 - 2. \quad (\text{C18})$$

From the “dual” relation for the four point function we know that $\alpha_4 + 2\alpha_3 - 2$ is the dominant term on the LHS of $\dot{\lambda}^{(4)}$ and therefore also on the RHS, i.e. in (C13). Hence, the inequality

$$\alpha_4 + 2\alpha_3 - 2 \leq 4\alpha_3 - 3 \quad (\text{C19})$$

necessarily holds. This inequality in turn implies $\alpha_4 \leq 2\alpha_3 - 1$, while (C18) is equivalent to $\alpha_4 \geq 2\alpha_3 - 1$. We conclude that

$$\alpha_4 = 2\alpha_3 - 1, \quad (\text{C20})$$

which is equivalent to the assumption $3\alpha_3 - 2 = \alpha_3 + \alpha_4 - 1$ while $3\alpha_3 - 2 < \alpha_3 + \alpha_4 - 1$ produces a contradiction.

With (C20) we have checked two of the three cases, i.e. under the \geq assumption only the $=$ sign is a consistent solution. The term involving α_5 is subject to the condition

$$\alpha_5 \geq \alpha_3 + \alpha_4 - 1. \quad (\text{C21})$$

Let us study the other case:

(ii) *Assume*

$$\alpha_3 + \alpha_4 - 1 < 3\alpha_3 - 2. \quad (\text{C22})$$

Comparing with (C12), we find that the equation for $\dot{\Gamma}^{(3h)}$ is trivially consistent with this assumption. Moreover, the assumption that $2\alpha_4 - 1$ is the leading term (which is equivalent to assumption (C22)) is consistent with the first three diagrams in (C13). Again, the terms involving α_5 and α_6 are appropriately constrained, see remark 2 below, and we can constitute that (C22) is indeed a consistent assumption. Including both cases, this leads to the relation

$$\alpha_4 \leq 2\alpha_3 - 1, \quad (\text{C23})$$

and proves the lemma. \square

Remark 1: This means that from $\dot{\Gamma}^{(3h)}$ and $\dot{\Gamma}^{(4h)}$ we obtain an inequality that constrains the relation between α_3 and α_4 , which are at this stage free parameters.

Remark 2: Lemma 1 with (C8) implies

$$\alpha_4 < 0 \quad (\text{C24})$$

always, thus α_3 cannot be constrained solely by the analysis above.

Remark 3: Moreover, we cannot fix α_n for $n > 4$ with the equations for the three- and the four-point function. However, since equations (C14) and (C15) are independent of α_4 and α_5 , these terms cannot be the leading contributions in the limit under consideration, i.e. they cannot generate the power law. This implies

$$\alpha_5 \geq \alpha_4 + \alpha_3 - 1. \quad (\text{C25})$$

Applying the same logic to the four-point function, we arrive at

$$\alpha_6 \geq 2\alpha_4 - 1. \quad (\text{C26})$$

In order to further constrain the parameters α_n with $n > 4$, we proceed by analyzing the running of $\Gamma^{(nh)}$.

Lemma 2: *Under the same conditions as in Lemma 1, we obtain the recursion relation for $n \geq 5$:*

$$\alpha_n = \alpha_{n-2} + \alpha_4 - 1. \quad (\text{C27})$$

Proof: In general, assumption (C9) together with (C11) leads to

$$\begin{aligned} \dot{\lambda}^{(n)} &\stackrel{\epsilon \rightarrow 0}{\sim} g \epsilon^{\alpha_n-1} \dot{\epsilon} \\ &\stackrel{\epsilon \rightarrow 0}{\sim} g \max \{ \epsilon^{\alpha_n+\alpha_4-1}, \epsilon^{\alpha_n+2\alpha_3-2} \}. \end{aligned} \quad (\text{C28})$$

The canonical term can be dropped since $\alpha_4 < 0$. Lemma 1 ensures that the leading term is always given by $\epsilon^{\alpha_n+\alpha_4-1}$. Accordingly, all terms generated by the diagrams on the RHS of the flow equation must be smaller or equal to this term. For every n , the flow equation for $\Gamma^{(nh)}$ contains a diagram with 2 four-point vertices, one

$1/\chi$	$\alpha_3 = -0.1$	$\alpha_3 = -0.2$	$\alpha_3 = -0.3$	$\alpha_3 = -0.4$	$\alpha_3 = -0.5$
10	$\mu_* = -0.645$ $g_* = 0.614$	$\mu_* = -0.651$ $g_* = 0.604$	$\mu_* = X$ $g_* = X$	$\mu_* = X$ $g_* = X$	$\mu_* = X$ $g_* = X$
15	$\mu_* = -0.630$ $g_* = 0.637$	$\mu_* = -0.633$ $g_* = 0.633$	$\mu_* = -0.637$ $g_* = 0.628$	$\mu_* = -0.641$ $g_* = 0.620$	$\mu_* = X$ $g_* = X$
20	$\mu_* = -0.624$ $g_* = 0.647$	$\mu_* = -0.626$ $g_* = 0.644$	$\mu_* = -0.628$ $g_* = 0.640$	$\mu_* = -0.630$ $g_* = 0.637$	$\mu_* = -0.634$ $g_* = 0.632$
25	$\mu_* = -0.621$ $g_* = 0.653$	$\mu_* = -0.622$ $g_* = 0.651$	$\mu_* = -0.623$ $g_* = 0.648$	$\mu_* = -0.625$ $g_* = 0.645$	$\mu_* = -0.627$ $g_* = 0.642$
30	$\mu_* = -0.618$ $g_* = 0.658$	$\mu_* = -0.619$ $g_* = 0.655$	$\mu_* = -0.621$ $g_* = 0.653$	$\mu_* = -0.620$ $g_* = 0.651$	$\mu_* = -0.623$ $g_* = 0.648$
35	$\mu_* = -0.617$ $g_* = 0.659$	$\mu_* = -0.618$ $g_* = 0.658$	$\mu_* = -0.619$ $g_* = 0.657$	$\mu_* = -0.620$ $g_* = 0.655$	$\mu_* = -0.621$ $g_* = 0.652$

TABLE VII: UV fixed point values for different parameters χ and α_3 with exponential regulator and $a = 4$. X indicates that no fixed point is found for these parameter values.

$(n-2)$ -vertex and 4 internal propagators. Hence, we can conclude

$$\alpha_n + \alpha_4 - 1 \leq 2\alpha_4 + \alpha_{n-2} - 2. \quad (\text{C29})$$

Moreover, we can generalize the results (C25) and (C26), by considering the diagram with only one vertex, more precisely, an $(n+2)$ -vertex. Again, consistency requires

$$\alpha_{n+2} \geq \alpha_n + \alpha_4 - 1 \quad (\text{C30})$$

or equivalently $\alpha_n \geq \alpha_{n-2} + \alpha_4 - 1$. Combining this result with (C29) proves lemma 2. \square

Remark 4: Lemma 2 yields a recursion relation connecting all α_n with α_4 and α_3 . We are therefore left with two free parameters, with the constraint (C24). Moreover, we can give explicit, non-recursive, expressions for α_n , depending on whether n is odd or even. The difference $\Delta\alpha$ between α_n and α_{n-2} is obviously

$$\Delta\alpha = \alpha_4 - 1, \quad (\text{C31})$$

and therefore independent of n . For n even we can express any α_n as

$$\begin{aligned} \alpha_n &= \alpha_4 + \left(\frac{n-4}{2}\right) \Delta\alpha \\ &= \left(\frac{n}{2} - 1\right) \alpha_4 - \left(\frac{n}{2} - 2\right), \quad n \text{ even}, n \geq 6, \end{aligned} \quad (\text{C32})$$

which can be rewritten as

$$\alpha_{2n} = (n-1)\alpha_4 - (n-2), \quad n \geq 3. \quad (\text{C33})$$

For n odd we can do the same thing, starting with α_3 and adding multiples of $\Delta\alpha$ in order to arrive at

$$\alpha_{2n+1} = \alpha_3 + (n-1)\alpha_4 - (n-1), \quad n \geq 2. \quad (\text{C34})$$

Appendix D: Estimating α_3

Following the argument in section III D, there is a transition regime between Einstein-Hilbert-type of solutions with $\lambda^{(2)} = \lambda^{(3)}$ and an IR regime where they differ as the trajectories approach $\epsilon = 0$. The simplest form of such a transition is a sharp switch between the two solutions at a scale k_0 when the trajectories bend over to the separatrix and are attracted towards the IR fixed point. Such a sharp cross-over between these two regions is certainly different from the true behaviour, and it also differs from our ansatz (35). However, this type of transition shares the essential features with the true solution and can thus provide a reasonable estimate. At the transition scale k_0 we have the connection conditions

$$\lambda^{(3)}(k_0) = \lambda^{(2)}(k_0) = -\frac{1}{2}\mu(k_0) \quad (\text{D1})$$

and

$$\dot{\lambda}^{(3)}(k_0) = \dot{\lambda}^{(2)}(k_0) = -\frac{1}{2}\dot{\epsilon}(k_0). \quad (\text{D2})$$

Using the power law (C6) we have the simple relation for the logarithmic derivative

$$\frac{(\lambda^{(3)})'}{\lambda^{(3)}} = \frac{\alpha_3}{\epsilon}, \quad (\text{D3})$$

where $'$ denotes the derivative with respect to ϵ . The scale derivative can be expressed as

$$\dot{\lambda}^{(3)} = \left(\lambda^{(3)}\right)' \dot{\epsilon}. \quad (\text{D4})$$

Evaluating the above equation at $k = k_0$ and combining it with (D2) yields

$$\left(\lambda^{(3)}\right)' \Big|_{k=k_0} = -\frac{1}{2}. \quad (\text{D5})$$

This in turn can be used together with (D2) when evaluating (D3) at $k = k_0$. Keeping in mind that $\epsilon = 1 + \mu$,

this results in

$$\alpha_3 = \frac{1 + \mu(k_0)}{\mu(k_0)}. \quad (\text{D6})$$

Together with $\alpha_4 = 2\alpha_3 - 1$ this fixes all α_n . From the phase diagram, one infers that the onset of this transition is near $\mu \approx -0.9$ independent of the chosen parameters. This gives

$$\alpha_3 \approx -1/9. \quad (\text{D7})$$

Not sticking to the equality does not alter the results qualitatively.

Appendix E: Functional form of $\lambda^{(n)}$

Here we construct explicit expressions for the functions $\lambda^{(n)}$. In addition to the singularity structure, there are further constraints to be fulfilled by such an ansatz. In the following we show that

$$\begin{aligned} \lambda^{(n)} &= -\frac{\mu}{2} \left[1 + \text{sgn}(\mu) \chi \left| \frac{\mu}{1 + \mu} \right|^{-\alpha_n} \right] \\ &= -\frac{\mu}{2} (1 + \delta\lambda^{(n)}) \end{aligned} \quad (\text{E1})$$

is consistent with all constraints. In the above formula χ is an arbitrary parameter. From perturbation theory we know that in the Gaussian limit $\mu \rightarrow 0$, we need to recover an Einstein-Hilbert solution. Indeed, (E1) entails $\lambda^{(n)} = -\mu/2$ for all n in the vicinity of $\mu = 0$ as long as $\alpha_n < 0$. In addition to that, it is clear that the correction cannot contain further powers of g , since this would interfere with the singularity structure. Furthermore, the correction should be inherently dimensionless. With these conditions, a quantity proportional to powers of the ratio $\mu/(1 + \mu)$ is everything we have at hand. In the end, we are left with two (constrained) free parameters, namely $\alpha_3 \leq 0$ and $\chi \in \mathbb{R} \setminus 0$. The proportionality factor χ is in general different for all $\lambda^{(n)}$ and can in principle be calculated from higher order vertex functions. In

our truncation we choose a uniform constant for simplicity. The IR structure is unaffected by the value of χ , but a large χ might alter the UV regime. Note that the scaling analysis is true in the IR limit only. Consequently, we expect a small χ which does not interfere with the UV regime.

Appendix F: Anomalous dimensions in the IR

Both anomalous dimensions need to vanish at the IR fixed point for it to be classical. For the ghost anomalous dimension, this is the case as long as $g/\epsilon \rightarrow 0$, which is equivalent to saying that $\alpha_3 < 0$, in accordance with our estimate above. On the other hand, the vanishing of the graviton anomalous dimension is seen as follows: First, as shown in [3], the terms quadratic in the external momentum in the flow cancel. Thus, the flow goes to a constant as the external momentum goes to infinity, and no divergences can appear there. Next, the flow equation for the mass can be rewritten as

$$\dot{\mu} = -2\mu + \frac{\partial_t \Gamma^{(2h)}(0)}{Z_h(0)} + \eta_h(0)\mu. \quad (\text{F1})$$

We know that in the IR for $\mu \rightarrow -1, g \rightarrow 0$, $\dot{\mu}$ vanishes. This can be achieved in 3 different ways: either the flow vanishes and the anomalous dimension at zero cancels the canonical scaling, or both the flow and the anomalous dimension cancel the canonical scaling, or only the flow remains finite. First assume that the flow vanishes in the limit $\mu \rightarrow -1, g \rightarrow 0$. We know that the leading order contribution comes from a term $\sim g\lambda^{(4)}$, all other terms have smaller divergences and thus vanish in the limit $g \rightarrow 0$. If this term vanishes, however, then the flow is 0 everywhere, thus also the anomalous dimension would vanish everywhere, and we would end up with no fixed point. On the other hand, assume that $g\lambda^{(4)}$ remains finite in our limit, then still all other terms in the flow vanish, and thus the flow is a nonzero constant. This in turn implies that the graviton anomalous dimension must vanish as it is a finite difference of the flow. We conclude that $\eta_h(p^2) = 0$ at the IR fixed point.

-
- [1] S. Weinberg, General Relativity: An Einstein centenary survey, Eds. Hawking, S.W., Israel, W; Cambridge University Press pp. 790–831 (1979).
 - [2] I. Donkin and J. M. Pawłowski (2012), 1203.4207.
 - [3] N. Christiansen, D. F. Litim, J. M. Pawłowski, and A. Rodigast, Phys.Lett. **B728**, 114 (2014), 1209.4038.
 - [4] M. Reuter, Phys. Rev. **D57**, 971 (1998), hep-th/9605030.
 - [5] D. F. Litim, Phys. Rev. Lett. **92**, 201301 (2004), hep-th/0312114.
 - [6] M. Niedermaier and M. Reuter, Living Rev.Rel. **9**, 5 (2006).
 - [7] R. Percacci (2007), to appear in 'Approaches to Quantum Gravity: Towards a New Understanding of Space, Time and Matter' ed. D. Oriti, Cambridge University Press, 0709.3851.
 - [8] A. Codello, R. Percacci, and C. Rahmede, Annals Phys. **324**, 414 (2009), 0805.2909.
 - [9] D. F. Litim, Phil.Trans.Roy.Soc.Lond. **A369**, 2759 (2011), 1102.4624.
 - [10] M. Reuter and F. Saueressig, New J.Phys. **14**, 055022 (2012), 1202.2274.
 - [11] S. Nagy (2012), 1211.4151.
 - [12] H. W. Hamber, Gen.Rel.Grav. **41**, 817 (2009), 0901.0964.
 - [13] J. Ambjorn, A. Goerlich, J. Jurkiewicz, and R. Loll,

- Phys.Rept. **519**, 127 (2012), 1203.3591.
- [14] J. Ambjorn, A. Goerlich, J. Jurkiewicz, and R. Loll (2013), 1302.2173.
 - [15] C. Wetterich, Phys.Lett. **B301**, 90 (1993).
 - [16] R. Percacci and D. Perini, Phys. Rev. **D67**, 081503 (2003), hep-th/0207033.
 - [17] J. E. Daum, U. Harst, and M. Reuter (2010), 1005.1488.
 - [18] A. Eichhorn and H. Gies (2011), 1104.5366.
 - [19] S. Folkerts, D. F. Litim, and J. M. Pawłowski, Phys.Lett. **B709**, 234 (2012), 1101.5552.
 - [20] U. Harst and M. Reuter, JHEP **05**, 119 (2011), 1101.6007.
 - [21] P. Donà, A. Eichhorn, and R. Percacci (2013), 1311.2898.
 - [22] T. Henz, J. M. Pawłowski, A. Rodigast, and C. Wetterich, Phys.Lett. **B727**, 298 (2013), 1304.7743.
 - [23] D. Benedetti, P. F. Machado, and F. Saueressig, Mod. Phys. Lett. **A24**, 2233 (2009), 0901.2984.
 - [24] K. Falls, D. Litim, K. Nikolakopoulos, and C. Rahmede (2013), 1301.4191.
 - [25] N. Ohta and R. Percacci, Class.Quant.Grav. **31**, 015024 (2014), 1308.3398.
 - [26] D. Benedetti, Europhys.Lett. **102**, 20007 (2013), 1301.4422.
 - [27] M. Demmel, F. Saueressig, and O. Zanusso (2014), 1401.5495.
 - [28] M. Shaposhnikov and C. Wetterich, Phys.Lett. **B683**, 196 (2010), 0912.0208.
 - [29] O. Antipin, J. Krog, M. Mojaza, and F. Sannino (2013), 1311.1092.
 - [30] K. Falls, D. F. Litim, and A. Raghuraman, Int.J.Mod.Phys. **A27**, 1250019 (2012), 1002.0260.
 - [31] K. Falls and D. F. Litim (2012), 1212.1821.
 - [32] B. Koch and F. Saueressig, Class.Quant.Grav. **31**, 015006 (2014), 1306.1546.
 - [33] B. Koch and F. Saueressig (2014), 1401.4452.
 - [34] D. F. Litim and T. Plehn, Phys. Rev. Lett. **100**, 131301 (2008), 0707.3983.
 - [35] E. Gerwick, D. Litim, and T. Plehn, Phys. Rev. **D83**, 084048 (2011), 1101.5548.
 - [36] S. Weinberg, Phys. Rev. **D81**, 083535 (2010), 0911.3165.
 - [37] E. J. Copeland, C. Rahmede, and I. D. Saltas (2013), 1311.0881.
 - [38] D. Litim and A. Satz (2012), 1205.4218.
 - [39] S. Nagy, J. Krizsan, and K. Sailer, JHEP **1207**, 102 (2012), 1203.6564.
 - [40] S. Rechenberger and F. Saueressig, Phys.Rev. **D86**, 024018 (2012), 1206.0657.
 - [41] C. Contreras and D. F. Litim (2014), in preparation.
 - [42] C. S. Fischer and J. M. Pawłowski, Phys. Rev. **D80**, 025023 (2009), 0903.2193.
 - [43] D. F. Litim and J. M. Pawłowski, World Sci. pp. 168–185 (1999), hep-th/9901063.
 - [44] J. Berges, N. Tetradis, and C. Wetterich, Phys. Rept. **363**, 223 (2002), hep-ph/0005122.
 - [45] K. Aoki, Int.J.Mod.Phys. **B14**, 1249 (2000).
 - [46] C. Bagnuls and C. Bervillier, Phys.Rept. **348**, 91 (2001), hep-th/0002034.
 - [47] J. Polonyi, Central Eur.J.Phys. **1**, 1 (2003), hep-th/0110026.
 - [48] J. M. Pawłowski, Annals Phys. **322**, 2831 (2007), hep-th/0512261.
 - [49] H. Gies, Lect.Notes Phys. **852**, 287 (2012), hep-ph/0611146.
 - [50] B.-J. Schaefer and J. Wambach, Phys.Part.Nucl. **39**, 1025 (2008), hep-ph/0611191.
 - [51] O. J. Rosten, Phys.Rept. **511**, 177 (2012), 1003.1366.
 - [52] J. M. Pawłowski, AIP Conf.Proc. **1343**, 75 (2011), 1012.5075.
 - [53] M. M. Scherer, S. Floerchinger, and H. Gies (2010), 1010.2890.
 - [54] J. Braun, J.Phys. **G39**, 033001 (2012), 1108.4449.
 - [55] W. Metzner, M. Salmhofer, C. Honerkamp, V. Meden, and K. Schönhammer, Reviews of Modern Physics **84**, 299 (2012), 1105.5289.
 - [56] I. Boettcher, J. M. Pawłowski, and S. Diehl, Nuclear Physics B Proceedings Supplements **228**, 63 (2012), 1204.4394.
 - [57] B. Delamotte, in *Lecture Notes in Physics, Berlin Springer Verlag*, edited by J. Polonyi and A. Schwenk (2012), vol. 852 of *Lecture Notes in Physics, Berlin Springer Verlag*, p. 49, cond-mat/0702365.
 - [58] J. M. Pawłowski, Acta Phys.Slov. **52**, 475 (2002).
 - [59] D. F. Litim and J. M. Pawłowski, JHEP **0209**, 049 (2002), hep-th/0203005.
 - [60] J. Braun, H. Gies, and J. M. Pawłowski, Phys.Lett. **B684**, 262 (2010), 0708.2413.
 - [61] A. Eichhorn, H. Gies, and M. M. Scherer, Phys.Rev. **D80**, 104003 (2009), 0907.1828.
 - [62] A. Eichhorn, Phys.Rev. **D87**, 124016 (2013), 1301.0632.
 - [63] F. Marhauser and J. M. Pawłowski (2008), 0812.1144.
 - [64] L. Fister and J. M. Pawłowski, Phys.Rev. **D88**, 045010 (2013), 1301.4163.
 - [65] A. Codello, G. D’Odorico, and C. Pagani (2013), 1304.4777.
 - [66] N. Christiansen, B. Knorr, J. M. Pawłowski, and A. Rodigast, in preparation (2014).
 - [67] J. A. M. Vermaseren (2000), arXiv:math-ph/0010025.
 - [68] J. Martingarcia, R. Portugal, and L. Manssur, Computer Physics Communications **177**, 640 (2007), 0704.1756.
 - [69] G. Guennebaud, B. Jacob, et al., *Eigen v3.2*, <http://eigen.tuxfamily.org> (2013).
 - [70] V. Branchina, K. A. Meissner, and G. Veneziano, Phys.Lett. **B574**, 319 (2003), hep-th/0309234.
 - [71] J. M. Pawłowski (2003), hep-th/0310018.
 - [72] D. F. Litim, Phys.Lett. **B486**, 92 (2000), hep-th/0005245.
 - [73] E. Manrique, M. Reuter, and F. Saueressig, Annals Phys. **326**, 463 (2011), 1006.0099.
 - [74] L. Fister and J. M. Pawłowski (2011), 1112.5440.
 - [75] A. Eichhorn and H. Gies, Phys. Rev. **D81**, 104010 (2010), 1001.5033.
 - [76] K. Groh and F. Saueressig, J. Phys. **A43**, 365403 (2010), 1001.5032.
 - [77] D. Schnoerr, I. Boettcher, J. M. Pawłowski, and C. Wetterich, Annals Phys. **334**, 83 (2013), 1301.4169.